PERGAMON

Journal of Structural Geology 26 (2004) 325–338

JOURNAL OF STRUCTURAL GEOLOGY

www.elsevier.com/locate/jsg

A mechanical model for multiply-oriented conjugate deformation bands

William A. Olsson[a,*], John C. Lorenz[b], Scott P. Cooper[b]

[a]*Geomechanics Department, MS 0751, Sandia National Laboratories, Albuquerque, NM 87185-0751, USA*
[b]*Geophysical Technology Department, MS 0750, Sandia National Laboratories, Albuquerque, NM 87185-0750, USA*

Received 5 April 2001; accepted 28 April 2003

Abstract

A unique suite of three pairs of conjugate deformation band sets is present in Jurassic sandstones in the southeastern corner of the San Juan basin, northwestern New Mexico. In order of sequential development, these conjugate pairs are oriented to form each of the three principal conjugate attitudes: (1) upright X's, (2) plan-view X's, and (3) recumbent X's. The symmetry axes of the three different X-geometries at this location are parallel, suggesting that the three systems are genetically related. A relatively simple stress history, with the horizontal stresses striking northeast and southeast and varying in magnitude but not in orientation, plausibly explains this suite of sequentially developed conjugate structures. In this model, the upright X's formed with dip-slip, normal offset under the initial conditions where the overburden was the maximum stress and the northeast-striking horizontal stress was the intermediate stress. Plan-view X's with strike-slip offset formed next, as the northeast-striking stress increased (due to northeastward Laramide translation of the Colorado Plateau and interaction with the local basement-cored Nacimiento Uplift) to become the maximum stress, leaving the overburden stress as the intermediate stress although unchanged in magnitude. As the northeast-directed horizontal compressive stress continued to increase, it eventually created a condition where the horizontal stresses equaled or exceeded the overburden stress, resulting in small-scale thrusting along the recumbent X's. The proposed mechanical model shows that shear stress levels dropped temporarily after the formation of the upright X's, providing a hiatus in deformation and making the deformation at the next stage distinct, without overlap. The three systems of intersecting conjugate deformation bands that resulted have severely compartmentalized potential reservoirs in this unit, and illustrate why similar high-porosity, deformation-banded units can have low hydrocarbon production rates despite otherwise good reservoir potential.
Published by Elsevier Ltd.

Keywords: Multiply-oriented conjugate deformation bands; Jurassic sandstones; Conjugate attitudes

1. Introduction

1.1. Statement of the problem

Three pairs of conjugate deformation bands occur in the sandy Westwater Canyon Member of the Jurassic Morrison Formation in the southeastern corner of the San Juan basin, near the village of San Ysidro, northwestern New Mexico (Fig. 1). We use Aydin's (1978) concept of deformation band as a very small fault with no surface of discontinuity. Crosscutting relationships allow the inference of the temporal evolution of the sets of deformation bands. The symmetry axes of the three conjugate systems of deformation bands are parallel despite the different basic orientations, suggesting that the systems are related. This suite of structures provides much closer constraints on the tectonic/stress history of the local area than are typically available for geologic problems. We interpret that history, as documented by this suite of stress indicators, and discuss how similar conjugate features may severely compartmentalize reservoirs with intersecting, low-permeability surfaces (Chapin et al., 2002; Shipton et al., 2002).

The presence of a conjugate pair of either deformation bands or shear fractures allows for the definitive reconstruction of the orientations of the three principal stresses present in the strata at the time of formation. In contrast, for extension fractures there is typically an ambiguity between the positions of the maximum and intermediate principal stresses (unless a definitive plume axis is present, e.g. Kulander et al., 1979). For deformation band (or shear fracture) pairs that clearly originated as conjugate systems: (1) the maximum compressive stress was normal to the line of intersection and directed along the line that bisects the

* Corresponding author. Tel. +1-505-844-7344; fax: +1-505-844-7354.
E-mail address: waolsso@sandia.gov (W.A. Olsson).

0191-8141/03/$ - see front matter Published by Elsevier Ltd.
doi:10.1016/S0191-8141(03)00101-9

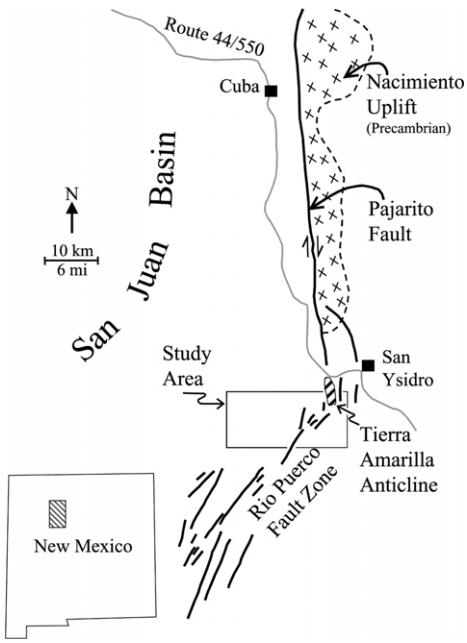

Fig. 1. Location map of study area.

acute conjugate angle, (2) the minimum compressive stress was normal to the line of intersection and oriented along the line that bisects the obtuse conjugate angle, and (3) the intermediate compressive stress coincided with the line of intersection of the two planes of the conjugate deformation band (shear fracture) pair (Fig. 2) (Anderson, 1942; Jaeger and Cook, 1969).

These relationships are useful in reconstructing the orientations of the stresses in the rock at the time of fracturing or deformation banding. For example, if a conjugate deformation band or shear fracture pair is oriented in the form of an upright X and is characterized by normal or dip-slip offset, then it can be concluded that the weight of the overburden provided the maximum compressive stress at the time of deformation banding or fracturing. If the conjugate X is recumbent (i.e. lying on its side), and offset was again dip-slip but with a reverse or thrust sense of motion then the weight of the overburden provided only the minimum stress. In each case, the orientations of all three stresses, and the relative stress magnitude in the vertical axis can be determined. These relationships are used below to reconstruct a plausible stress history during the formation of a unique system of conjugate deformation bands.

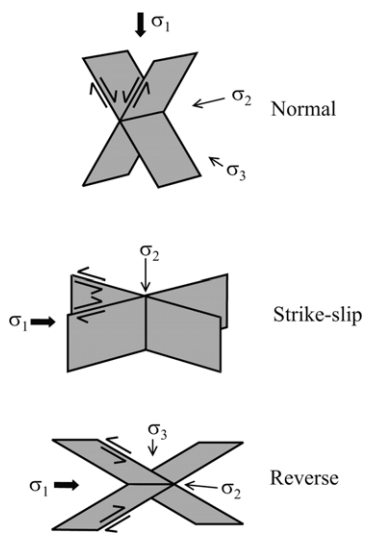

Fig. 2. Orientation of deformation bands and sense of shear as in Anderson's (1942) theory of faulting. Top = 'upright' (normal offset), middle = 'plan view' (strikeslip offset), bottom = 'recumbent' (reverse or thrust offset) X's.

1.2. General setting

1.2.1. Structure

The San Ysidro area is located in the southeastern corner of the San Juan basin, lying immediately south and west of the southern termination of the basement-cored, block-faulted Nacimiento uplift, and within the northern end of the Rio Puerco Fault Zone. Normal faults in this area, striking approximately NE–SW, were superimposed onto broad, asymmetric, north to northwest striking folds (Figs. 1 and 3). The folds are generally considered to have formed during latest Cretaceous time (early Laramide deformation) whereas the faults are considered to be of Eocene age (late Laramide events) (Baltz, 1967; Woodward et al., 1972, 1992; Woodward, 1987). Many of the faults were reactivated by extension in mid-Miocene time during formation of the Rio Grande rift, and now have up to 30 m of normal offset.

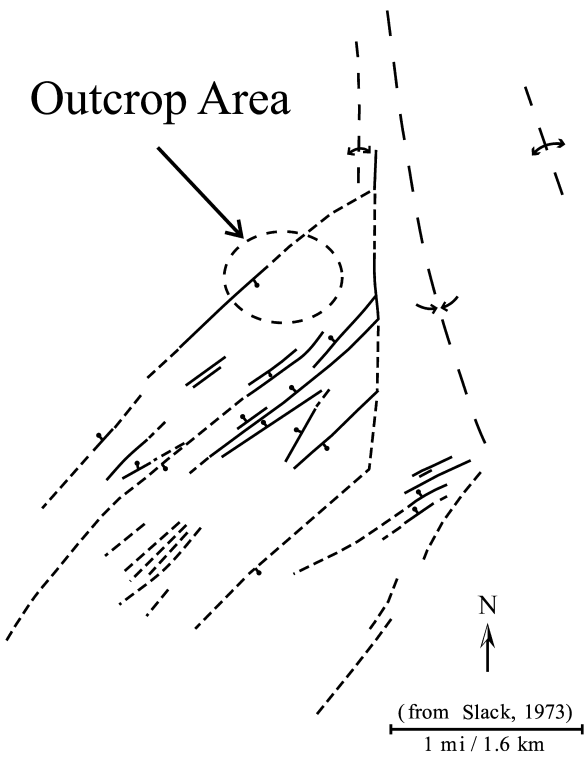

Fig. 3. Enlargement of faulted area in Fig. 1.

Large-scale (tens of meters to kilometers) structures within and surrounding the Nacimiento Uplift have been used to reconstruct the local kinematics of the area, and are summarized here as constraints on the formation of the San Ysidro deformation bands. The large-scale structures record northeastward translation of the Colorado Plateau, including the San Juan basin on its eastern edge, during the Laramide Orogeny. Varying amounts of right-lateral offset have been reconstructed at the eastern boundary of the plateau at this time (Woodward et al., 1972; Chapin and Cather, 1981, 1983; Cather, 1999). These structures also suggest that an early stage of broad-scale, low-amplitude uplift in the area of the Nacimiento Mountains was followed by right-lateral wrench faulting along the N–S striking Pajarito fault that marks the western edge of the uplift.

The Pajarito fault was originally interpreted to be a thrust fault with a suggested 1–1.5 km of westward motion by Renick (1931), although more recent authors have differed on interpretation. The fault is inferred to have accommodated as much as 5 km of right-lateral offset as well as 3 km of stratigraphic offset (Baltz, 1967; Woodward et al., 1972). Erslev (2001) has reinterpreted the area to suggest that right-lateral wrench offset during Laramide time was minimal. The Pajarito fault dies out southward in the vicinity of the Tierra Amarilla anticline, the largest structure in the San Ysidro study area, where the reported stratigraphic throw has diminished to about 25 m and where evidence for strike-slip offset is absent or obscured. This marks the transition from the Nacimiento Uplift region to the Rio Puerco Fault Zone (Figs. 1 and 3), where a band of en échelon, N–E-striking normal faults has been interpreted to be the surface expression of both E–W extension and right-lateral wrench faulting at the basement level (Slack and Campbell, 1976).

The San Ysidro structural domain described here lies in this transitional zone. The Tierra Amarilla Anticline probably marks the southernmost basement faults of the Nacimiento Uplift, and the local NE–SW striking faults are the most northerly normal faults of the Rio Puerco Fault Zone. Thus the deformation bands described here formed in an overall system of regional NE–SW compression related to Laramide translation of the Colorado Plateau, complicated by local NE–SW striking normal faults and N–S wrench faults. The deformation bands may have been the local strain-accommodation mechanism in these Jurassic strata for the Laramide events that created N–S to NE–SW striking vertical extension fractures in Cretaceous strata throughout the rest of the San Juan basin (Lorenz and Cooper, 2001, 2003).

1.2.2. Stratigraphy of the host strata

The deformation bands described in this study occur in the Westwater Canyon Member, and locally in the Upper Member, of the Jurassic Morrison Formation (Fig. 4). Overlying Triassic and older Jurrassic strata, the Morrison Formation varies from 230 to 290 m thick (Slack, 1973) and is composed of nonmarine fluvial and overbank sandstones

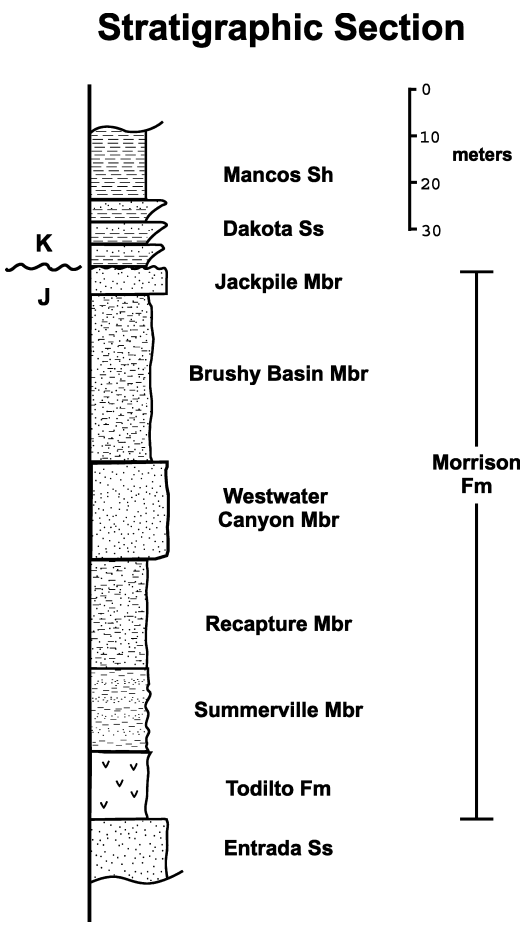

Fig. 4. Simplified stratigraphic section for study area. Deformation bands discussed here are found in the Westwater Canyon Member of the Morrison Formation.

and mudstones (Ruetschilling, 1973; Slack, 1973; Woodward and Schumacher, 1973). The cliff-forming Westwater Canyon (Fig. 5) is 50 m thick, and consists of generally friable, crossbedded, arkosic sandstones. The sandstones are generally coarse grained but range from fine- to coarse-grained and contain local conglomeratic lenses. The 20-m-thick Upper Member is composed of friable, medium-grained, whitish sandstones (Schlee and Moench, 1961; Woodward and Schumacher, 1973), and is unconformably overlain by the Dakota Sandstone and Mancos Shale.

1.3. Background on deformation bands

Intersecting shear fractures that have opposite senses of motion can reasonably be called conjugate fractures if the offset motion is demonstrably penecontemporaneous. Ideal conjugate fracture pairs have an acute apical angle (roughly 60°) that was bisected by the maximum compressive stress at the time of fracturing (e.g. Anderson, 1942). Deformation bands are roughly planar features that record some small amount of displacement, typically a few centimeters to less than a millimeter, and can be viewed as small-displacement faults, or as coherent shear fractures (Aydin, 1978; Aydin

Fig. 5. Cliff-forming Westwater Canyon Member shown in foreground. Nacimiento uplift is on the horizon.

and Johnson, 1983; Antonellini et al., 1994; Mair et al., 2000). Rather than being discontinuous features like fractures, deformation bands typically have measurable widths (commonly less than a millimeter), and consist of broken and compacted sand grains that define the shear band. Larger amounts of displacement can be accommodated by wide zones of multiple, composite deformation bands (Aydin, 1978; Aydin and Johnson, 1983; Antonellini et al., 1994). Deformation bands typically form in high-porosity, poorly cemented sandstones. Conjugate systems of deformation bands have been observed in the field (Antonellini et al., 1994; Davis, 1999; Cooper, 2000; Herrin, 2002) including in the San Juan basin (Lorenz and Cooper, 2000), and in the laboratory (Friedman and Logan, 1973; Olsson, 2000).

Antonellini et al. (1994) described three major groupings of deformation bands: (1) deformation bands with no cataclasis, (2) deformation bands with cataclasis, and (3) deformation bands with clay smearing. Group 1 deformation bands are further subdivided into bands displaying (a) dilatancy, (b) no volume change, or (c) porosity reduction (compaction). Under specific conditions deformation bands can be formed by early, transient dilatancy during grain boundary sliding followed by pore collapse (group 1) and grain breakage (group 2) (Antonellini et al., 1994). Petrographic observations of grain breakage within deformation bands at San Ysidro suggest that they fall within Antonellini et al.'s (1994) group 2, although the San Ysidro bands are not concentrated near faults as described by Antonellini et al. (1994), but rather are distributed across the outcrop much like group 1 deformation bands.

Conjugate fracture patterns have been reported elsewhere in the San Juan basin, although typically only as pairs in one orientation and nowhere else in such abundance. Whitehead (1997) reported N–S striking, upright conjugate pairs in outcrops of Tertiary strata in the northwestern part of the basin, and Lorenz et al. (1999) reported subsurface evidence for plan-view conjugate fractures in siliceous sandstones of the Dakota Formation in several parts of the basin. Lorenz and Cooper (2000) also report recumbent conjugate fractures in Dakota sandstones that crop out at the northern and northeastern edges of the San Juan basin. The orientations of the axes of these conjugate fracture pairs suggest that they are related to more regional, basin-wide stresses, and they do not appear to be directly related to the deformation bands described here.

2. The intersecting conjugate deformation band systems at San Ysidro

The three distinct pairs or systems of deformation bands in the San Ysidro structural domain are each oriented with their symmetry axes normal and parallel to bedding, and the symmetry axes of the three systems are coaxial though interchangeable. These deformation band pairs are extremely well exposed in three dimensions in outcrop. The main outcrop covers most of about 0.5 km^2, where hummocky erosion has cut into the top of the high-porosity, poorly cemented, coarse sandstones of the Westwater Canyon Member of the Jurassic Morrison Formation. The deformation bands are exposed in essentially unlimited lateral dimensions and up to 3 m in the vertical dimension. The vertical dimension is further augmented where several small canyons cut through to the base of the 50-m-thick sandstone. Examination of other exposures several kilometers in all directions from this main outcrop confirm that this pattern is in fact regional.

Thin sections of the deformation bands show sequential and alternate development of intersecting planes (Figs. 6 and 7). Since the intersecting planes did not develop simultaneously, there is no volume reduction or compaction at the points of intersection.

Petrographic examination shows that many of the ductile

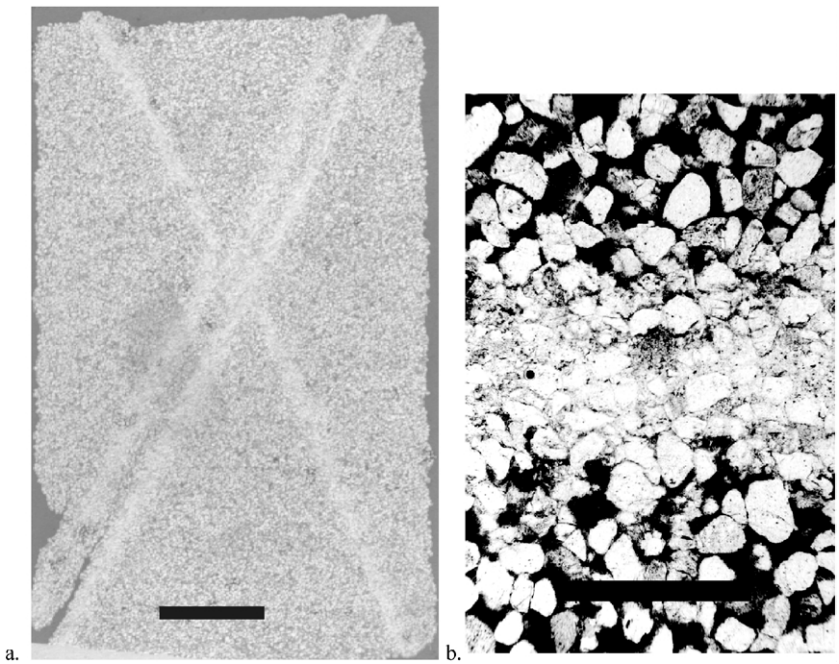

Fig. 6. (a) Thin section of deformation bands showing sequential rather than contemporaneous development of three shear bands of the earliest, normal conjugate pair. Scale bar = 5 mm. (b) Close up of thin section in (a), showing pseudomatrix of crushed rock fragments and other weaker grains filling porosity between quartz grains in band. The deformation band is the horizontal, lighter shaded zone at the midline of the specimen. Scale bar = 1 mm.

and labile rock fragments have been turned into a pseudomatrix within the band. Labile grains comprise 30–40% of the distinct sand grains outside the band but they comprise only 5–10% of the distinct grains within the band. The rest of these grains have been disaggregated into a matrix that occludes nearly all of the porosity within the band. Individual quartz grains are essentially the same size within the bands, but they are not significantly closer together within the bands than outside the bands; the pseudomatrix fills the porosity between grains within the bands. Many of the corners have been broken off quartz and feldspar grains within the deformation bands, so that they have become more rounded than their equivalents in the adjacent matrix rock (Fig. 6b).

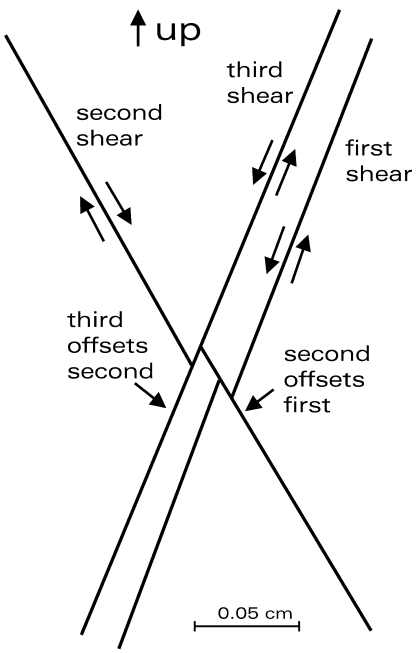

Fig. 7. Line drawing of the deformation bands shown in Fig. 6a. Senses of shear and timing of shearing is indicated.

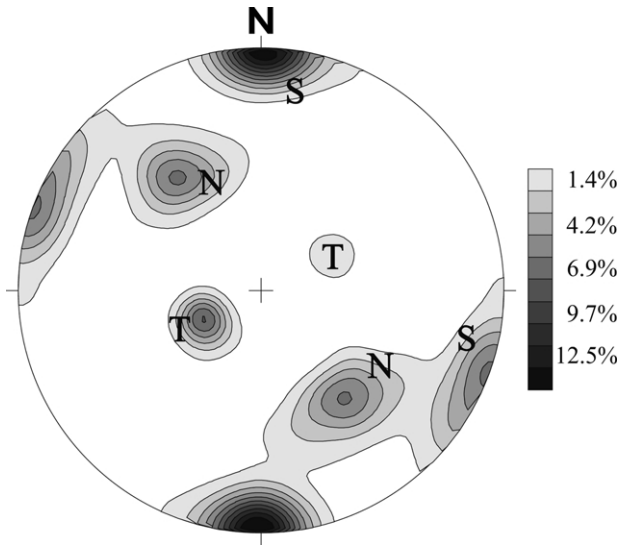

Fig. 8. Stereogram of angular density of poles to deformation bands in the Jurassic Morrison formation plotted in lower hemisphere. Contours are by the method of Kamb (1959). Normal deformation bands indicated by N, strike-slip bands by S, and thrust bands by T. There are 360 poles represented on the plot. The scale bar gives percentage of points per unit area.

A summary stereogram of angular pole density for 360 deformation bands measured in outcrop, plotted in the lower hemisphere and contoured by the method of Kamb (1959), is shown in Fig. 8. This figure shows the high degree of definition, as indicated by the clear separations between maxima, of the three systems of deformation bands. The first-formed system (Fig. 8, N) is represented by the northeast striking system of bands that dip both to the southeast and the northwest. The second-formed system of bands is indicated by maxima for vertical planes striking about 20 and 90° (Fig. 8, S). The last-formed system of bands is indicated by the maxima for planes striking about 140° and dipping both to the northeast and the southwest (Fig. 8, T).

2.1. System 1

Based on intersecting and offsetting relationships, the oldest system of deformation bands is oriented as an upright 'X'. The acute-angle bisector of this X is bed-normal (within 7° of vertical) and the deformation-band planes strike northeast, dipping about 60° to either the southeast or northwest. Textbook X's occur where the bands are spaced relatively closely (Fig. 9), but isolated planes and meter-scale zones of parallel planes that are inclined in only one of the two dip directions are also common. Each band may occur singly or may be a composite of several subparallel, inosculating (Aydin, 1978; Davis, 1999) bands. The bands typically extend the entire length and height of any given outcrop (several meters) but are limited vertically by larger sedimentary bedding breaks.

Spacing of this first system of deformation bands varies from less than a centimeter to several meters. Observable offsets on the bands are rare because there are few correlation layers within this massive sandstone and offsets are small. However, normal, dip-slip offsets of up to several millimeters can locally be documented where individual, opposite-dipping members of this pair intersect. Northwest-dipping bands and southeast-dipping bands are offset by each other in approximately equal numbers, and local compound examples even show alternating offsets (Figs. 6 and 7). This system of deformation bands is ubiquitous within the thicker, high-porosity Jurassic sandstones, but such inclined planes are not present in other parts of the local stratigraphic column.

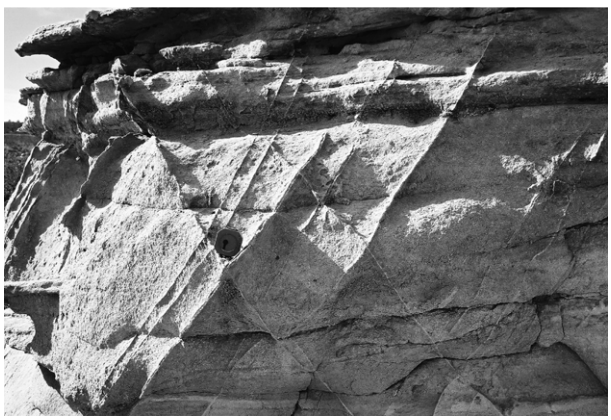

Fig. 9. Typical example of the normal deformation bands; both sets of the system are represented. Pocket transit at band intersection for scale.

It has been established that the two sets of bands forming this system occurred simultaneously and they have been sheared in the sense of shortening in the direction of the acute bisector. Therefore, they are small normal faults, or normal deformation bands (Aydin, 1978). Henceforth, we refer to this system of bands as *normal bands* (N, Fig. 8; also Fig. 9).

2.2. System 2

Plan-view conjugate 'X' patterns of deformation bands (Fig. 10) were formed next, as demonstrated by local offset of the earlier bands by several millimeters where they intersect. These bands are oriented normal to bedding and the members of the pair strike north-northeast (with right-lateral offsets) and east (with left-lateral offsets). The acute-angle bisector is parallel to bedding, striking northeast. As with the first conjugate system, the ideal X geometry is not universal: isolated deformation bands, and zones where only one of the two members of the pair occur as parallel bands,

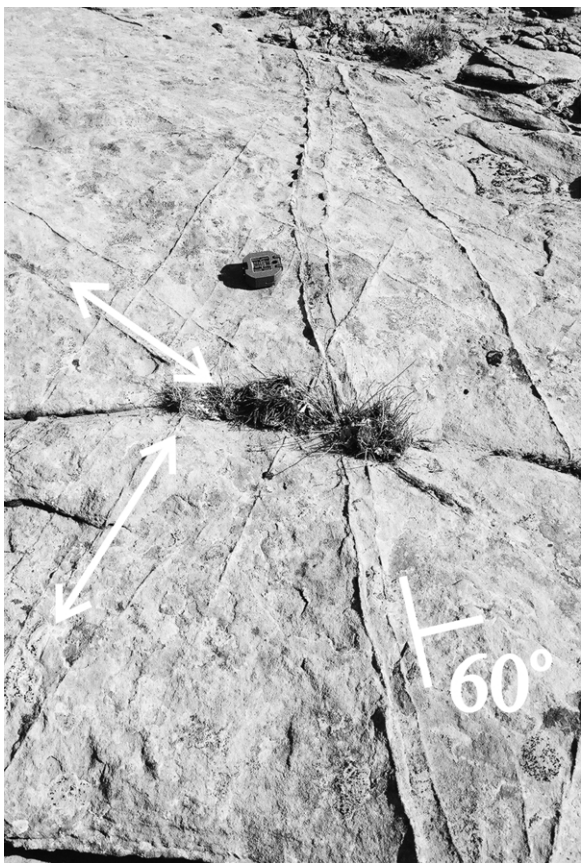

Fig. 10. Bedding plane exposure of both sets of the strike-slip system (double-ended arrows) and several members of one set of the normal system (dipping 60° to southeast. Pocket transit for scale.

are mixed with domains where the more ideal, intersecting conjugate pairs are present.

In addition to the obvious geometric reorientation of these bands from the first system, there are other differences. The overall surface of this second system of deformation bands is composed of en échelon segments typically 10 cm to a meter in length (faintly visible in Fig. 10). The segments strike within 3–4° of parallel to the overall trend of the plane, and are always oriented counterclockwise to the overall trend of the east-striking bands (stepping to the right) and clockwise to the overall trend of the north-northeast-striking bands (stepping left). Another difference is that the bands comprising this conjugate system are typically singular, with few compound, inosculating bands such as are common in the earlier normal conjugate pair. The spacing of the bands within the second system of deformation bands is similar to that of the first system.

This second conjugate system of deformation bands is common throughout the high-porosity Westwater Canyon sandstones. Interestingly, it mimics the most common system of orientations for fractures and deformation bands in other parts of the local stratigraphic column, particularly the overlying sandstones of the Dakota Formation, although the systems are not perfectly parallel.

Orientations and senses of shear indicate that these bands are equivalent to small-scale strike-slip faults. Henceforth, we refer to this system as *strike-slip bands* (S, Fig. 8).

2.3. System 3

The third, and youngest system of conjugate deformation bands is not as pervasive as the older systems. Although this recumbent system of bands is present locally over large areas, and is common at certain horizons and at certain locations, it is not ubiquitous within the same zones where the earlier two systems are widespread. One area where this system is as common as the other two systems is in a 2-m-thick sandstone several meters above the top of the Westwater Canyon Member, west of the northeast-striking normal fault that cuts through the area. It has also been found within the sandstones at the top of the Westwater Canyon Member several hundred meters east of the fault, and within several thinner, better cemented sandstones higher in the section.

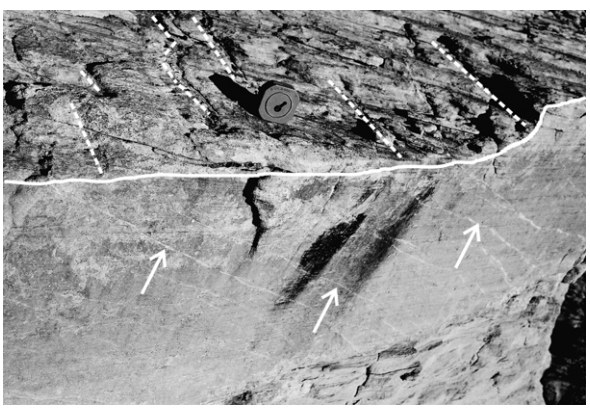

Fig. 11. Bedding surface (above crooked white line) and vertical cliff face (below crooked white line) of one set of thrust bands. Dotted lines drawn near several of the bedding surface exposures. Arrows point to several of the cross-sections. Pocket transit for scale.

Deformation bands of this youngest system strike northwest, and dip at low angles, about 30° to bedding, towards the northeast and southwest (Fig. 11). Sense and magnitudes of offset are typically obscure, although local offsets and geometry suggest reverse offset. Offset appears to be on the order of millimeters. The bands are single and irregular, not segmented and arranged en échelon as are those of system 2, nor compound and inosculating as are many of the system 1 bands. Where present, the system 3 bands tend to be relatively closely spaced (less than a meter). Domains of isolated bands, as well as domains where the parallel bands of only one member of the system dominate the rock, are common.

Orientations, senses of shear and relative timing suggest that these bands are equivalent to a system of small-scale conjugate thrust faults; thus we refer to them as *thrust bands* (T, Fig. 8; Fig. 11).

3. Mechanical model for the origin of the three coexistent conjugate systems of deformation bands

In this section we use an assumed failure condition and a particular set of boundary conditions to describe the origin of the three systems of conjugate deformation bands. Upon first consideration, it may seem that fairly complicated rotations and changes in magnitudes of the components of the stress tensor would be required to form the three systems with the observed timing and distinct separations of maxima on the pole density diagram (Fig. 8). We will show, however, that increasing vertical stress accompanying

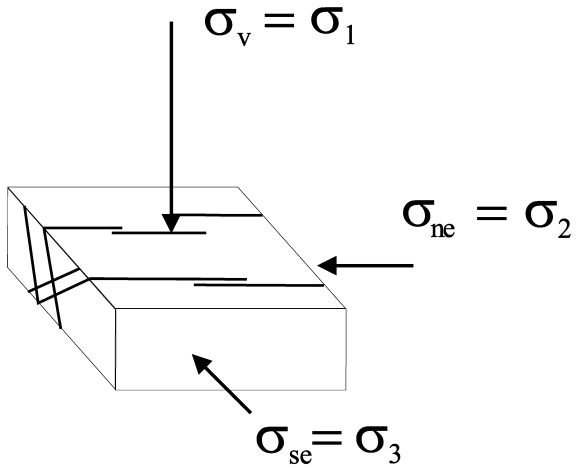

Fig. 12. Block diagram suggesting the relationship between the normal bands and the stress system required for their formation. Figs. 15 and 16 show stress state at the beginning and ending of normal banding.

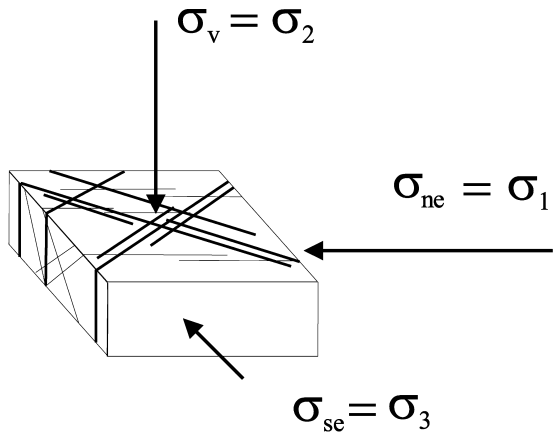

Fig. 13. Block diagram suggesting the relationship between the strike-slip bands and the stress system required for their formation and showing the beginning of three-dimensional compartmentalization. Correlative to end of Stage 3—Fig. 18.

sedimentary loading, combined with a continued, tectonically-driven increase of one of the horizontal principal stresses, is a simple stress history that can result in the sequential development of all three systems of conjugate shear bands.

Our conceptual model of the banding history and the causative stresses is outlined in Figs. 12–14. Each successive episode of deformation banding overprinted the existing bands with the result that the Westwater Canyon is divided into small compartments bounded by deformation bands.

The failure of rocks by fracture in terms of stress state has long been described by the Coulomb–Mohr criterion (e.g. Hubbert, 1951; Jaeger and Cook, 1969; Twiss and Moores, 1992). To the extent that the Coulomb–Mohr criterion actually represents any given set of data, it can be useful because it also predicts the orientation of the fracture with respect to the stress tensor. (In the linear case, the criterion is simply the Coulomb criterion.) Thus two separate elements

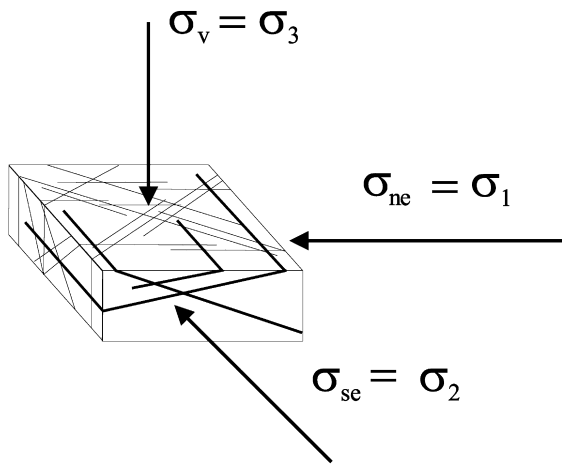

Fig. 14. Block diagram suggesting the relationship between the thrust bands and the stress system required for their formation and showing the final three-dimensional compartmentalization. Correlative to Stage 4—Fig. 19.

are represented in Mohr's stress space: a failure criterion and the magnitude and orientation of any stress tensor.

We assume the material to be non-hardening and that the failure condition in terms of shear stress τ and normal stress σ on a particular plane is linear, such that:

$$\tau = c + \mu\sigma \tag{1}$$

where c is the cohesion and μ is the coefficient of internal friction. Restricting the stress–strain response to being non-hardening is tantamount to fixing the Coulomb line to prevent its movement in Mohr space. An alternative measure of the slope of the failure condition is the angle of internal friction ϕ defined by $\phi = \arctan \mu$. Following the usual rock mechanics convention that compression is positive and the principal stresses are ordered as $\sigma_1 > \sigma_2 > \sigma_3$, shear stress τ and normal stress σ are:

$$\tau = \tfrac{1}{2}(\sigma_1 - \sigma_3)\sin 2\theta \tag{2}$$

$$\sigma = \tfrac{1}{2}(\sigma_1 + \sigma_3) + \tfrac{1}{2}(\sigma_1 - \sigma_3)\cos 2\theta \tag{3}$$

These expressions involve the maximum principal stress difference $\sigma_1 - \sigma_3$, which is the diameter of the circle whose center is located at $(\sigma_1 + \sigma_3)/2$. Cyclic interchange of the subscripts generates two other circles, to which we will refer, for the remaining two principal stress differences, $\sigma_2 - \sigma_3$ and $\sigma_1 - \sigma_2$.

The assumption of no strain hardening applies to the homogeneously deforming phase (outside of the bands) of the material only and will be found to be an important constraint on the model to be developed. The material within individual bands does strain harden, however (Mair et al., 2000), possibly because of the intense shear strain in these thin layers. This strain hardening allows only a small amount of shear offset to take place across a given band.

The material data, c and μ, for the Coulomb criterion are unavailable for the sandstone of the Westwater Canyon Member but can be estimated as follows. The acute apical angles for each of the three systems of deformation bands range from 60 to 70°. For simplicity we chose $\theta = 60°$ to be representative. A standard relation for Coulomb failure (Hubbert, 1951) is $\theta = \pm(\pi/4 + \phi/2)$, which gives $\phi = 30°$ and $\mu = 0.58$. The implication of the $\pm$ sign is that there are two symmetrically disposed bands; we use only the positive part of the Mohr plane in this paper, but explicitly accept that there are two possible, conjugate, bands for each failure state. Thus for the simple Coulomb criterion, the conjugate angles of the deformation bands themselves gives one of the constitutive parameters, ϕ, the slope of the failure line.

Having ϕ in hand, it is only necessary to choose the cohesion. To estimate this parameter we turn to the paper by Dunn et al. (1973) in which they give strength data for a number of sandstones of varying porosities. Their data gives $c \approx 25$ MPa and $\phi = 30°$ for sandstones having porosities of from 12 to 17%. Thus we took as representative for this problem $c = 25$ MPa and $\phi = 30°$.

When studied in detail, within the framework of a

particular boundary value problem, outlined below, the Coulomb criterion exposes a novel phenomenon in the successive deformation banding (or faulting) of rock under simply changing stress states. For continuous changes in the vertical stress and one horizontal principal stress, distinct successive failure states can be achieved to form the three systems of deformation bands at San Ysidro.

We propose that the three discrete systems of deformation bands can be explained by the response of a body of rock subjected to two superposed states of stress: one related to a subsiding sedimentary basin with loading in the vertical direction, and another resulting from an increasing horizontal tectonic stress. We use a right-handed coordinate system ('se'; 'ne'; 'v') with 'se' pointing southeast, 'ne' pointing northeast, and 'v' pointing upward. Thus σ_{se} represents the principal compressive stress acting along the horizontal line trending SE–NW, σ_{ne} represents the principal compressive stress at a right angle, acting along a horizontal, NE–SW trend, and σ_v acts along the vertical.

It is also necessary to account for the presence of pore fluids, assumed to be water, to determine the effective stresses that control deformation (e.g. Jaeger and Cook, 1969). For total vertical stress σ^t_{ij} due to the weight of overlying water-saturated rock, effective stresses are $\sigma_{ij} = \sigma^t_{ij} - p\delta_{ij}$, where δ_{ij} is the Kronecker delta. We assume for simplicity that p is simply $\rho_w g d$, where ρ_w is the density of water, g is acceleration due to gravity, and d is depth of burial. This assumption ignores the possibility that the zone of interest is either overpressured or underpressured with respect to the hydrostatic gradient.

The assumption of zero horizontal strain is commonly made to estimate the state of stress at depth (Price, 1966). The vertical effective stress is taken to be $\sigma_v = \rho g d$, where $\rho = \rho_r \rho_w$ and ρ_r is density of dry rock. Then for the baseline elastic problem of no lateral strain in terms of effective stresses, $\epsilon_{ne} = \epsilon_{se} = 0$ and

$$\sigma_{se} = \sigma_{ne} = \frac{\nu}{1-\nu}\sigma_v \tag{4}$$

where ν is Poisson's ratio. For many sandstones $0.1 < \nu < 0.25$ (Jaeger and Cook, 1969).

The additional tectonic stress σ_t directed NE–SW can be modeled as the plane strain system (Jaeger and Cook, 1969)

$$\sigma_{ne} = \sigma_t; \qquad \epsilon_{se} = 0; \qquad \sigma_v = 0 \tag{5}$$

Superimposing these two systems gives, for the total state of stress:

$$\sigma_v = \rho g d \tag{6}$$

$$\sigma_{ne} = \frac{\nu}{1-\nu}\sigma_v + \sigma_t \tag{7}$$

$$\sigma_{se} = \frac{\nu}{1-\nu}\sigma_v + \nu\sigma_t \tag{8}$$

The set of Eqs. (4)–(8) constitute the elastic part of the problem solved to investigate the sequential development of the observed systems of deformation bands. Solutions to this set of equations require knowledge of the constitutive parameter ν and boundary data in the sense of stress history.

The maximum stress circle has a unique point on its perimeter defined by its intersection with the radius $2\theta = \pi/2 + \phi$. The locus of points satisfying the definitions of σ and τ as given by Eqs. (2) and (3) for the chosen value of $\theta = 60°$ defines the stress path. It will be shown that the stress path is piecewise linear in Mohr space and that each segment is related to a phase of either elastic deformation or differing banding activity, and can be characterized by its slope. This is found in each segment by differentiating Eqs. (2) and (3) to find:

$$d\sigma = \tfrac{1}{2}(d\sigma_1 + d\sigma_3) + \tfrac{1}{2}(d\sigma_1 - d\sigma_3)\cos 2\theta \tag{9}$$

$$d\tau = \tfrac{1}{2}(d\sigma_1 - d\sigma_3)\sin 2\theta \tag{10}$$

As the problem evolves, the geographic stresses σ_{se}, σ_{ne}, and σ_v alternately become the different values σ_1, σ_2, and σ_3.

3.1. Stage 1

We start with sedimentation and burial that caused loading in the vertical direction. Initially, $\sigma_v = \sigma_{se} = \sigma_{ne} = 0$. At some small depth corresponding to the time of cementation the material becomes elastic. With increasing sedimentation and depth of burial, σ_v increases and consequently according to Eq. (4) so do both horizontal stresses. Because the deformation bands have a well-defined orientation (the line of intersection of the two sets is 55°), σ_{ne} must have been at least marginally larger than σ_{se} at the time of banding. Thus, in the absence of contraindicating information, it was assumed that σ_t began to contribute to σ_{ne} early on so that there would be sufficient difference between σ_{ne} and σ_{se} to orient the normal bands. The difference was assumed to be about 1 MPa.

During Stage 1, both σ_v and σ_t increased, due to continued sedimentation and tectonic activity, respectively, (σ_t proportionately much slower) until the failure condition was reached. Setting $\sigma_v = \sigma_1$ and $\sigma_{se} = \sigma_3$ in Eqs. (9) and (10), and eliminating the minimum stress using Eq. (4) gives:

$$d\sigma = \frac{1}{2}d\sigma_v\left(\frac{1}{1-\nu}\right) + \frac{1}{2}d\sigma_v\left(\frac{1-2\nu}{1-\nu}\right)\cos 2\theta \tag{11}$$

$$d\tau = \frac{1}{2}d\sigma_v\left(\frac{1-2\nu}{1-\nu}\right)\sin 2\theta \tag{12}$$

The slope of the stress path for $\theta = 60°$ and $\nu = 0.15$ is

$$\frac{d\tau}{d\sigma} = 0.933$$

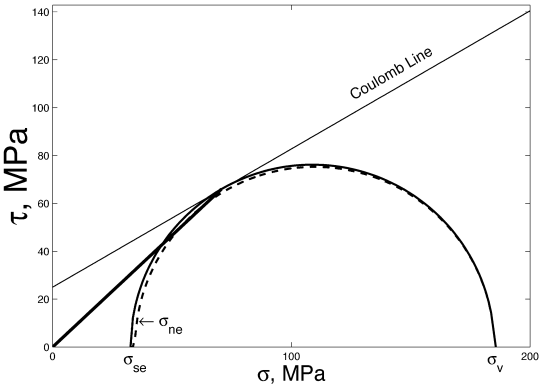

Fig. 15. Stage 1: Axisymmetric, elastic loading. The solid circle is $\sigma_v - \sigma_{se}$. The dotted circle is $\sigma_v - \sigma_{ne}$. The circle for $\sigma_{ne} - \sigma_{se}$ is too small to see.

or 43°. During initial vertical loading (Fig. 15), the stress circle expanded and moved to the right simultaneously, with minimum σ_{se} and maximum σ_v related by Eq. (4). Fig. 15 shows a set of stress circles for the last point of the elastic loading segment, at the failure stress, i.e. at the point of tangency of the circle with the Coulomb line. By the time failure occurred, the $\sigma_v - \sigma_{ne}$ circle (dotted) just becomes visible. The $\sigma_{se} - \sigma_{ne}$ circle is too small to be seen at the scale of the drawing. The slope of the stress path is controlled by the values of ν and θ. Stage 1 is terminated by the development of the normal deformation bands when the stress path intercepts the failure condition. Stage 1 can be characterized as (nearly) axisymmetric elastic loading to the failure line. The line of intersection of the two sets was oriented NE–SW because σ_{ne} was just larger than σ_{se} and assumed the role of σ_2.

It is easily found that as $\nu \rightarrow 0$ the slope of the stress path approaches 60°. As $\nu \rightarrow 0.5$, the slope of the path goes to 0°. For $\nu \geq 0.25$ the stress path lies parallel to or below the Coulomb line and thus failure by normal banding cannot occur. The very existence of the normal bands then implies that $\nu < 0.25$, and in turn that the rock was probably cemented when banding occurred. That is, the bands at San Ysidro are not soft sediment deformation in the uniaxial strain environment. Normal bands could, however, form in soft sediment in an extensional environment.

3.2. Stage 2

In the absence of strain hardening, a further increase in σ_v could have been accommodated by the maximum stress circle continuing to increase and moving to the right, but with σ_{se} and σ_v then related by μ. That is, the further motion of the maximum stress circle is constrained to move in contact with the failure line. Continued generation of new normal bands could take place because a given band sheared only a fixed small amount and then other bands, with higher nucleation stresses, formed at higher shear stresses. Strain hardening of bands has been described in the experimental context by Mair et al. (2000).

To find how the circles evolved while in contact with the failure line we used the general linear relation between σ_1 and σ_3 in terms of the Coulomb parameters (e.g. Hubbert, 1951; Jaeger and Cook, 1969):

$$\sigma_1 = 2c\tan\theta + \tan^2\theta\sigma_3. \tag{13}$$

Differentiating and replacing σ_1 with σ_v and σ_3 with σ_{se} gives the slope of the new segment of stress path:

$$\mathrm{d}\sigma_v = \tan^2\theta\sigma_{se}. \tag{14}$$

For $\theta = 60°$ this results in $\mathrm{d}\sigma_{se} = 0.333\mathrm{d}\sigma_v$. The segment is shown as a thick line that coincides with the Coulomb line (Fig. 16).

The horizontal, tectonic increment of stress may have been driven by large-scale movements of tectonic plates, such that σ_{ne} continued to increase. The cessation of sedimentation corresponding to increasing depth of burial marked the end of Stage 2 and transition to Stage 3, wherein tectonic loading continued. There is insufficient geologic information to specify precisely the maximum σ_v for this problem so the length of the stress path segment that coincides with the failure line is unknown. Apart from the difference between σ_{se} and σ_{ne} required to maintain the systematic alignment of normal bands, the loading during Stage 2 was, as for Stage 1, axisymmetric and plastic along the failure line up to the arbitrarily selected end of the normal banding process.

3.3. Stage 3

During Stage 3, tectonic loading continued, and thus σ_{ne} grew in magnitude. The vertical stress σ_v was then stationary, as sedimentation had ceased, and therefore σ_{ne} became the driving stress. The tectonic stress may have been related to the same source that caused overthrusting along the nearby Nacimiento Uplift. Increasing σ_t in Eqs. (7) and (8) while holding σ_v fixed ($\sigma_v = \rho g d_{final}$) yields the interesting and fundamentally important result that the

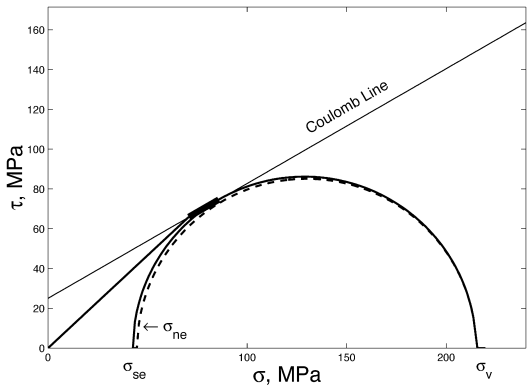

Fig. 16. Stage 2: Condition during the formation of normal bands: nearly axisymmetric loading along failure line. The stress path increment is the heavy short line coincident with the Coulomb line. The solid circle, $\sigma_v - \sigma_{se}$, portrays the end of Stage 2. The dotted circle gives the $\sigma_v - \sigma_{ne}$ stress; the $\sigma_{ne} - \sigma_{se}$ circle is very small and cannot be seen (see Fig. 12).

stress path began to drop below the failure condition even while two stress components, σ_{ne} and σ_{se}, continued to increase, and the third remained constant, bringing to a close further normal deformation banding. As σ_{ne} increased, it pulled σ_{se} along with it, through the coupling exhibited in Eqs. (7) and (8). The vertical stress σ_v remained constant. Therefore the maximum circle, $\sigma_v - \sigma_{se}$, *receded* from contact with the failure line. This resulted in biaxial, elastic unloading. The decreasing linear segment of the stress path results from the elastic relationship of σ_{se} to σ_{ne}. Noting that $\sigma_v = \text{const.}$ and hence $d\sigma_v = 0$, Eqs. (9) and (10) reduce, after eliminating σ_{se} with Eqs. (7) and (8), to:

$$d\sigma = \tfrac{1}{2}\nu d\sigma_{ne} - \tfrac{1}{2}\nu d\sigma_{ne}\cos 2\theta \quad (15)$$

$$d\tau = -\tfrac{1}{2}\nu d\sigma_{ne}\cos 2\theta. \quad (16)$$

Insertion of numerical values gives $d\tau/d\sigma = -0.573$ or a slope of $-29°$. When σ_{ne} first equaled σ_v this downward trend ceased. This segment is referred to as Stage 3a and is illustrated in Fig. 17.

A second distinct segment of this stage began as σ_{ne} exceeded σ_v, whereupon σ_{ne} became the maximum principal stress and the maximum circle was $\sigma_{ne} - \sigma_{se}$. Now $d\sigma_v = 0$ and $d\sigma_{se} = \nu d\sigma_{ne}$. Using this data in Eqs. (9) and (10) yields:

$$d\sigma = \tfrac{1}{2}[1 + \nu + (1 - \nu)\cos 2\theta]d\sigma_{ne} \quad (17)$$

$$d\tau = \tfrac{1}{2}(1 - \nu)\sin 2\theta d\sigma_{ne} \quad (18)$$

that in turn results in $d\tau/\sigma = 1.0154$, an inclination of 45.4°. Thus Stage 3b was brought to a close by the stress path again meeting the Coulomb failure condition, but then, as the stresses were ordered $\sigma_{ne} > \sigma_v > \sigma_{se}$, strike slip style deformation bands were the preferred mode of deformation. The stress path was extended linearly up to the failure line (Fig. 18). Stage 3b was essentially biaxial, elastic loading.

3.4. Stage 4

Similar to the period following the onset of normal banding, here again, the driving stress, σ_{ne}, continued to increase. The maximum stress circle was again constrained to remain in contact with the Coulomb failure line as it expanded and moved to the right. The slope of the stress path was the same as in Stage 2. Throughout the stage, the stresses were ordered $\sigma_{ne} > \sigma_v > \sigma_{se}$ and gave rise to continued strike slip banding. As σ_{ne} increased, it caused σ_{se} to increase according to Eq. (8). Thus σ_{se} approached σ_v from the left and, eventually, $\sigma_{se} = \sigma_v$ (Fig. 19).

At this point, for an isotropic, homogeneous material, subjected to uniform boundary conditions, the two equivalent major stress circles $\sigma_{ne} - \sigma_v$ and $\sigma_{ne} - \sigma_{se}$ were equally likely to cause thrust bands and strike slip bands, respectively. Thus it appears that both thrust and strike-slip bands could form simultaneously with continued tectonic displacement. Closer examination, however, shows that only thrust banding was allowed.

First, consider shear banding driven by $\sigma_{ne} - \sigma_{se}$. The biaxial strain condition implies that any strike slip shearing will increase σ_{se} above σ_v. As a result, the maximum stress circle becomes $\sigma_{ne} - \sigma_v$ and the condition for strike slip

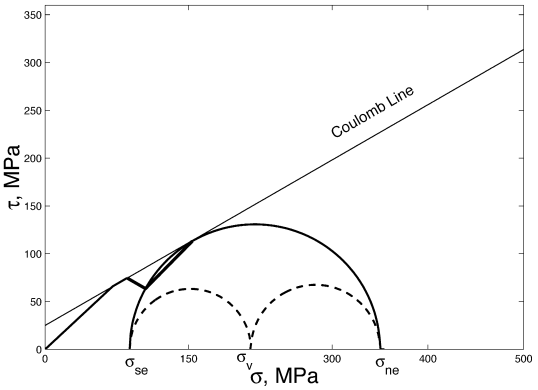

Fig. 18. Stage 3b: Biaxial elastic loading conditions during last part of quiescent interlude. The solid circle and its two internal dotted circles show the point at which the stress path intersects the Coulomb line. Strike slip bands form at this time (see Fig. 13).

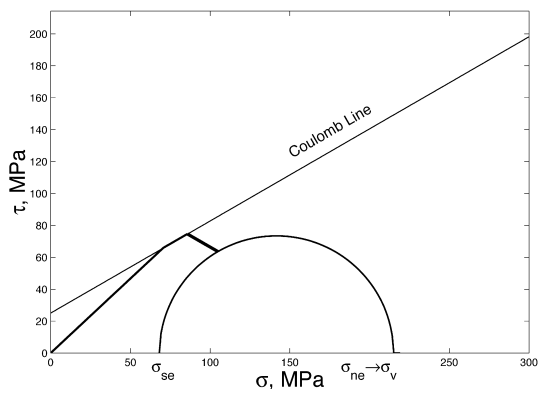

Fig. 17. Stage 3a: Biaxial elastic unloading conditions during first part of quiescent interlude. The solid circle, $\sigma_v - \sigma_{se}$, shows end of Stage 3a. The $\sigma_v - \sigma_{ne}$ circle is equivalent.

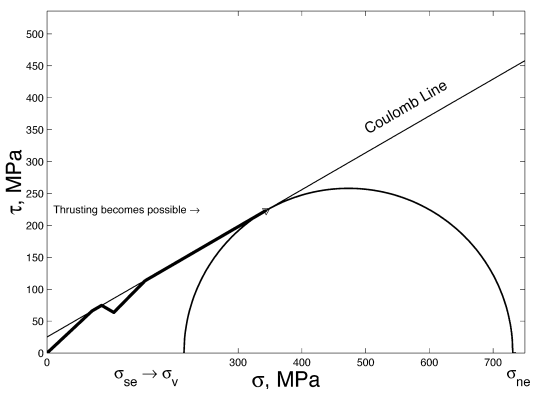

Fig. 19. Stage 4: Biaxial loading along the Coulomb line until $\sigma_{se} \rightarrow \sigma_v$. At this point, the solid circle, $\sigma_{ne} - \sigma_{se} = \sigma_{ne} - \sigma_v$, shows stresses at beginning of potential thrust banding (see Fig. 14).

failure is no longer satisfied. Second, thrust failure, driven by $\sigma_{ne} - \sigma_v$, is possible but σ_v is fixed. With one point of the Mohr circle, σ_v, determined, the non-hardening assumption fixes the other stress σ_{ne}. Thus, in the San Ysidro area, further strike slip banding was inhibited and thrust banding must have occurred at fixed σ_v and σ_{ne}.

Stresses of tectonic origin are displacement driven, and the stress σ_{ne} could have remained constant while continuing tectonic deformation was absorbed by the formation of thrust bands. Thus, it seems that thrust banding at the exclusion of strike slip banding could have continued indefinitely at this point. This emphasizes the fact that Mohr stress space does not indicate anything about the kinematics of deformation.

The relative paucity of thrust bands in the study area suggests that the source of σ_{ne} abated soon after the initiation of the thrust band system.

4. Discussion

We are unaware of many geologic settings where a similar suite of sequential conjugate patterns records the tectonic stress history. One possible example is in the area of the Emigrant Gap Anticline in Natrona County, Wyoming, where Beck and Burford (1985) documented patterns of strike-slip and thrust conjugate pairs similar to conjugate systems 2 and 3 in the San Ysidro area. No preliminary, normal conjugate X's equivalent to system 1 are present to record an early stress where the overburden was the maximum in Wyoming, and the conjugate patterns are apparently not as easy to discern at the small scale of individual outcrops as they are at San Ysidro. However, two systems of extension fractures, oriented parallel to the plane defined by their respective associated conjugate-pair intersection and the acute-angle bisectors, also occur in this system. Beck and Burford (1985) have used this fracture system to empirically infer a stress history similar to that reconstructed here for the San Ysidro area.

The three conjugate systems described in this paper are not universal in strata of the San Ysidro area. Large-scale, northeast-striking normal faults cut the entire succession, and may be equivalent to the early, normal conjugate band system (Stage 1). An apparently conjugate system of bed-normal, strike-slip fracture/deformation band planes is present in the younger, cleaner Dakota sandstones, but the strikes of these features (10–20° and 60–70°) are somewhat oblique to the Morrison strike-slip system. In fact, the 10–20° set in the overlying Dakota sandstone is remarkably similar to the vertical extension fracture strikes noted in most of the rest of the San Juan basin (Lorenz and Cooper, 2001). It may be that these existed in the rock as extension fractures but were reactivated in shear with the development of a younger, 60–70° set of shear planes to form a conjugate set with a slightly different orientation. No thrust faults or other indications of lifting of the overburden compatible with the thrust-related, third system of conjugate deformation bands are apparent in the San Ysidro area.

It appears that the different strata in the San Ysidro area had different mechanical properties, and thus different susceptibilities to fracturing and/or the formation of deformation bands. Brittle strata like the cleaner Dakota sandstones were fractured early and often with vertical extension fractures under an early NNE–SSW compression, whereas the higher-porosity Morrison strata in the same area display no record of this strain. However, the Morrison strata contain a definitive record of NE–SW compression that may also be expressed in the NE–SW normal faults of the area, but that is ambiguous in the Dakota strata.

The Laramide orogeny, extending from latest Cretaceous through Eocene time, was the first tectonic event to influence the San Juan basin following deposition of the Morrison and Dakota strata studied here. Regional, base-of-the-crust traction is inferred to have dragged the Colorado Plateau northeastward, providing a mechanism for near-surface deformation and the creation of the localized, basement-block Laramide uplifts (e.g. Woodward et al., 1972; Bird, 1998). Most of the strain in the nearby San Juan basin consists of pervasive N–S to NNE–SSW striking fractures, inferred to have been caused by Laramide displacement of the San Juan and Zuni Uplifts, north and south of the basin, respectively, toward each other with the San Juan basin caught between (Lorenz and Cooper, 2001, 2003). However, the San Ysidro area was peripheral to this system, located in the extreme southeastern corner of the basin, and the local conjugate deformation bands show that the maximum horizontal compressive stress in this area was oriented NE–SW. Currently there is discussion as to the Laramide kinematics and sense(s) of motion along the Nacimiento front. Cather (1999) and Woodward et al. (1972), among others, suggest that minimal westward thrusting followed an episode of significant right-lateral offset (up to 33 km proposed). Erslev (2001) and Pollock et al. (1998) believe that Laramide motion along this front has been almost entirely W – SW vergent thrusting. The deformation bands described in this paper could be viewed as consistent with either interpretation. Late Laramide overthrusting along the Nacimiento front would have been a probable source of NE–SW compression in the San Ysidro area, resulting in compression of the strata between that front and the northeastward indentation of the Zuni Uplift to the southwest, as proposed by Chamberlin and Anderson (1989).

Conjugate patterns of one or more orientations may have either positive or negative effects on a reservoir. Intersecting conjugate fractures, where minimal shear offset has created enhanced permeability pathways along the fracture planes, will provide a network of intersecting permeability that can significantly improve the three-dimensional conductivity and connectivity within a reservoir (Lorenz, 1997). However, if shear offset along these same fractures has

exceeded a certain threshold, that permeability network may be damaged irreparably (Olsson and Brown, 1993), and the resulting plumbing system of the reservoir begins to resemble that of one dominated by low-permeability deformation bands.

Reservoir conductivity across a deformation band may be reduced from that of the adjacent matrix by up to three orders of magnitude (Antonellini and Aydin, 1995; Fossen and Hesthammer, 1998; Chapin et al., 2002; Shipton et al., 2002; Holcomb and Olsson, 2003). A single system of conjugate deformation bands will reduce reservoir conductivity in the directions normal to the members of the conjugate pair, leaving a pronounced permeability anisotropy in the reservoir. Recent work by Chapin et al. (2002) shows that the degree of permeability anisotropy in the plane normal to the axis of intersection of the two members in a conjugate pair of deformation bands is a function of the dihedral angle. The greatest value of the permeability in such a system is that of the matrix, and is oriented parallel to the conjugate intersection axis.

However, when one or more systems of differently oriented, conjugate deformation-band pairs are superimposed on each other such as in the San Ysidro area, the reservoir becomes severely compartmentalized as system permeability is reduced to the value of that normal to the bands in all directions. In the San Ysidro Jurassic sandstones, the compartments are typically on the order of centimeters to several meters across, meaning that despite high porosity and good oil saturations, any similar reservoir would be difficult if not impossible to produce economically. In effect it would require drilling a well to drain each meter-scale compartment. Such unproducible reservoirs do in fact exist, and have been reported anecdotally from the Nubian Sandstone of Egypt (Tim Harper, personal communication, 1985), and from sandstone reservoirs in offshore Nigeria (Laird Thompson, personal communication, 2000).

5. Summary

Three intersecting systems of conjugate deformation bands are present in the Jurassic strata of the Morrison area. These deformation bands can be interpreted most easily in terms of a northeast-striking horizontal tectonic compressive stress that ramped up over time in response to the development of larger-scale structures. The northeast/southwest-directed compressive stress σ_{ne} initially constituted the intermediate stress, while the overburden/vertical stress σ_v was the maximum stress. Sometime after failure occurred in the form of a set of normal, dip-slip, conjugate deformation shear bands, the effective shear stress level dropped due to the influence of the intermediate principal stress on the system. With continued tectonic development of the area, σ_{ne} increased to become the maximum compressive stress, the unchanged overburden stress became the intermediate stress, and the effective shear stress level again developed to the magnitude necessary for failure. At this point, strike-slip conjugate shear-band developed. The final stage was reached when the Poisson effect dictated that the σ_{se}, without changing orientation, increased such that the unchanged overburden stress was equaled or exceeded by σ_{se}. At this point, the overburden was lifted along thrust-oriented, conjugate deformation-band planes. The resulting pattern of intersecting, low-permeability deformation bands in the high-porosity, high-permeability, Morrison strata has reduced the overall system permeability in all three directions to well below that of the matrix. Economic production of hydrocarbons from such a reservoir would be nearly impossible.

Acknowledgements

This work was supported by the U.S. Department of Energy's Office of National Petroleum Technology, Paul West, program manager. Sandia is a multiprogram laboratory operated by Sandia Corporation, a Lockheed Martin Company, for the United States Department of Energy under contract DE-ACO4-94AL85000.

References

Anderson, E.M., 1942. The Dynamics of Faulting and Dyke Formation with Application to Britain, Oliver and Boyd, Edinburgh, London.

Antonellini, M.A., Aydin, A., 1995. Effect of faulting on fluid flow in porous sandstones: geometry and spatial distribution. American Association of Petroleum Geologists Bulletin 79, 642–671.

Antonellini, M.A., Aydin, A., Pollard, D.D., 1994. Microstructure of deformation bands in porous sandstones at Arches National Park, Utah. Journal of Structural Geology 16, 941–959.

Aydin, A., 1978. Small faults formed as deformation bands in sandstone. Pure and Applied Geophysics 116, 913–930.

Aydin, A., Johnson, A.M., 1983. Analysis of faulting in porous sandstones. Journal of Structural Geology 5, 19–31.

Baltz, E.H., 1967. Stratigraphy and regional tectonic implications of part of upper Cretaceous and Tertiary rocks, east-central San Juan basin, New Mexico. U.S. Geological Survey Professional Paper 552.

Beck, W.C., Burford, A.E., 1985. Stress Analysis of the Casper Mountain-Emigrant Gap Anticline juncture, Natrona County, Wyoming. Thirty-sixth Annual Field Conference, Wyoming Geological Association Guidebook, pp. 59–65.

Bird, P., 1998. Kinematic history of the Laramide orogeny in latitudes 35°–49° N, western United States. Tectonics 17, 780–801.

Cather, S.M., 1999. Implications of Jurassic, Cretaceous, and Proterozoic piercing lines for Laramide oblique-slip faulting in New Mexico and rotation of the Colorado Plateau. Geological Society of America Bulletin 111, 849–868.

Chamberlin, R.M., Anderson, O.J., 1989. The Laramide Zuni Uplift, southeastern Colorado Plateau: a microcosm of Eurasian-style indentation-extrusion tectonics? In: Anderson, O.J., Lucas, S.G., Love, D.W., Cather, S.M. (Eds.), Southeastern Colorado Plateau, New Mexico Geological Society 40th Annual Field Conference Guidebook, pp. 81–90.

Chapin, C.E., Cather, S.M., 1981. Eocene tectonics and sedimentation in the Colorado Plateau–Rocky Mountain area. In: Dickinson, W.R.,

Payne, M.D. (Eds.), Relations of Tectonics to Ore Deposits in the Southern Cordillera. Arizona Geological Society Digest 14, pp. 173–198.

Chapin, C.E., Cather, S.M., 1983. Eocene tectonics and sedimentation in the Colorado Plateau–Rocky Mountain area. In: Lowell, J.D., Gries, R. (Eds.), Rocky Mountain Foreland Basins and Uplifts. Rocky Mountain Association of Geologists, pp. 33–56.

Chapin, J.R., Sternlof, K.R., Pollard, D.D., Durlofsky, L.J., 2003. Permeability effects of systematic deformation band arrays in sandstone. 2003 AAPG Annual Convention, Salt Lake City, p. 43.

Cooper, S.P., 2000. Deformation within a basement-cored anticline: Teapot Dome, Wyoming. M.Sc. thesis, New Mexico Institute of Mining and Technology, Department of Earth and Environmental Science, Socorro, NM.

Davis, G., 1999. Structural geology of the Colorado plateau region of southern Utah, with special emphasis on deformation bands. Geological Society of America, Special Paper 342.

Dunn, D.D., LaFountain, L.J., Jackson, R.E., 1973. Porosity dependence and mechanism of brittle fracture in sandstones. Journal of Geophysical Research 78, 2403–2417.

Erslev, E.A., 2001. Multistage, multidirectional Tertiary shortening and compression in north-central New Mexico. Geological Society of America Bulletin 113, 63–74.

Fossen, H., Hesthammer, J., 1998. Deformation bands and their significance in porous sandstone reservoirs. First Break 16, 21–25.

Friedman, M., Logan, J.M., 1973. Lüders' bands in experimentally deformed sandstone and limestone. Geological Society of America Bulletin 84, 1465–1476.

Herrin, J.M., 2002. Characteristics of deformation bands cutting poorly lithified sand: Rio Grande Rift, New Mexico. M.Sc. thesis, New Mexico Institute of Mining and Technology, Department of Earth and Environmental Science, Socorro, NM.

Holcomb, D.J., Olsson, W.A., 2003. Compaction localization and fluid flow. Journal of Geophysical Research, 108(B6):2290. (doi: 10.1029/2001JB000813, 2003).

Hubbert, M.K., 1951. Mechanical basis for certain familiar geologic structures. Bulletin Geological Society America 62, 366–372.

Jaeger, J.C., Cook, N.G.W., 1969. Fundamentals of Rock Mechanics, 2nd ed, Chapman and Hall, London.

Kamb, W.B., 1959. Ice petrofabric observations from Blue Glacier, Washington, in relation to theory and experiments. Journal of Geophysical Research 64, 1891–1919.

Kulander, B.R., Barton, C.C., Dean, S.L., 1979. The application of fractography to core and outcrop fracture investigations. METC/SP-79/3, Morgantown Energy Technology Center, Morgantown, W. Va., 174pp.

Lorenz, J.C., 1997. Conjugate fracture zones: potential "sweet spot" reservoirs within regional parallel-fracture systems. Paper 38749, Society of Petroleum Engineers, Annual Technical Conference, San Antonio, TX.

Lorenz, J.C., Cooper, S.P., 2000. Tectonic setting and characteristics of natural fractures in Mesaverde and Dakota reservoirs of the San Juan Basin, New Mexico and Colorado. In: Teufel, L.W., Engler, T. (Eds.), Optimization of Infill Drilling in Naturally-fractures Tight-gas Reservoirs of the San Juan Basin. A Final Report for the U.S. Department of Energy and Industry Cooperative Agreement DEFC26-98FT40486, pp. 2.1–2.84.

Lorenz, J.C., Cooper, S.P., 2001. Tectonic setting and characteristics of natural fractures in Mesaverde and Dakota reservoirs of the San Juan Basin, New Mexico and Colorado. Sandia National Laboratories Technical Report, SAND2001-0054.

Lorenz, J.C., Cooper, S.P., 2003. Tectonic setting and characteristics of natural fractures in Mesaverde and Dakota reservoirs of the San Juan Basin, New Mexico and Colorado, New Mexico. Geology, 25 No. 1, 3–14.

Lorenz, J.C., Basinski, P.M., Head, C.F., Peabody, W.W., 1999. Complex natural fracture patterns in Dakota Sandstone reservoirs of the San Juan Basin. San Antonio, TX. American Association of Petroleum Geologists, Annual Meeting Expanded Abstracts.

Mair, K., Main, I., Elphick, S., 2000. Sequential growth of deformation bands in the laboratory. Journal of Structural Geology 22, 25–42.

Olsson, W.A., 2000. Origin of Lüders' bands in deformed rock. Journal of Geophysical Research 105, 5931–5938.

Olsson, W.A., Brown, S.R., 1993. Hydromechanical response of a fracture undergoing compression and shear. International Journal of Rock Mechanics and Mining Sciences 30, 845–851.

Pollock, C.J., Stewart, K.G., Wallace, L.M., 1998. Structural model of the Sierra Nacimiento Uplift, north-central New Mexico, and the amount of dextral slip along part of the Nacimiento fault system. Geological Society of America, Abstracts with Programs, 30.

Price, N.J., 1966. Fault and Joint Development, Pergammon, Oxford.

Renick, B.C., 1931. Geology and ground-water resources of western Sandoval County, New Mexico. United States Geological Survey Water-Supply Paper 620.

Ruetschilling, R.L., 1973. Structure and stratigraphy of the San Ysidro Quadrangle, Sandoval County. MSc thesis, University of New Mexico.

Schlee, J.S., Moench, R., 1961. Properties and genesis of the "Jackpile" sandstone, Laguna, New Mexico. In: Peterson, J.A., Osmond, J.C. (Eds.), Geometry of Sandstone Bodies, American Association of Petroleum Geologists, Tulsa, pp. 134–150.

Shipton, Z.K., Evans, J.P., Robeson, K.R., Forster, C.B., Snelgrove, S., 2002. Structural heterogeneity and permeability in faulted eolian sandstone: implications for subsurface modeling of faults. American Association of Petroleum Geologists 86, 863–883.

Slack, P.B., 1973. Structural geology of the northeast part of the Rio Puerco fault zone, Sandoval County, New Mexico. M.Sc. thesis, University of New Mexico.

Slack, P.B., Campbell, J.A., 1976. Structural geology of the Rio Puerco fault zone and its relationship to central New Mexico Tectonics. In: Woodward, L.A., Northrop, S.A. (Eds.), Tectonics and Mineral Resources of Southwestern North America, New Mexico Geological Society Special Publication 6, pp. 46–52.

Twiss, R.J., Moores, E.M., 1992. Structural Geology, W.H. Freeman, New York.

Whitehead, N.H. III, 1997. Fractures at the surface, San Juan Basin, New Mexico and Colorado. In: Hoak, T.E., Klawitter, A.L., Blomquist, P.K. (Eds.), Fractured Reservoirs: Characterization and Modeling Guidebook, Rocky Mountain Association of Geologists, pp. 27–42.

Woodward, L.A., 1987. Geology and mineral resources of Sierra Nacimiento and vicinity, New Mexico, Memoir 42, New Mexico Bureau of Mines and Mineral Resources.

Woodward, L.A., Schumacher, O.L., 1973. Morrison Formation of southeastern San Juan basin, New Mexico. New Mexico Bureau of Mines and Mineral Resources, Circular 129.

Woodward, L.A., Kaufman, W.H., Anderson, J.B., 1972. Nacimiento fault and related structures, northern New Mexico. Geological Society of America Bulletin 83, 2383–2396.

Woodward, L.A., Hultgren, M.C., Crouse, D.L., Merrick, M.A., 1992. Geometry of Nacimiento–Gallina fault system, northern New Mexico. In: Lucas, S.G., Kues, B.S., Williamson, T.E., Hunt, A.P. (Eds.), San Juan Basin IV. New Mexico Geological Society Guidebook, 43rd Field Conference, pp. 103–108.